BMB
Reports

BMB Rep. 2026; 59(4): 242-252
www.bmbreports.org

Comparative analyses of ChIP-seq, CUT&RUN and CUT&Tag for Polycomb chromatin profiling

Yoonji Oh[1,#], Hanbyeol Kim[1,#], Sanghyun Lee[2], Soon-Jung Park[3], Yun-Gwi Park[3], Sung-Hwan Moon[3], Inkyung Jung[2] & Chul-Hwan Lee[1,4,5,]*

[1]Department of Biomedical Sciences and Pharmacology, Seoul National University College of Medicine, Seoul 03080, [2]Department of Biological Sciences, KAIST, Daejeon 34141, [3]Department of Animal Science and Technology, Chung-Ang University, Anseong 17546, [4]Cancer Research Institute, Ischemic/hypoxic Disease Institute, Medical Research Center, Seoul National University, Seoul 03080, [5]Wide River Institute of Immunology, Seoul National University, Hongcheon 25159, Korea

Chromatin profiling methods such as ChIP-seq, CUT&RUN, and CUT&Tag differ substantially in background structure, signal distribution, and resolution, complicating direct quantitative comparison across platforms. In this study, we systematically compared conventional and double-crosslink ChIP-seq, CUT&RUN, and CUT&Tag by profiling the Polycomb-associated histone modification H3K27me3 in human cardiomyocytes and the PRC2 catalytic subunit EZH2 in pluripotent stem cells. To enable cross-assay comparison, we developed a biologically informed normalization strategy based on stable Polycomb reference loci, allowing harmonization of signal scales while preserving assay-intrinsic signal architecture. This approach revealed CUT&RUN to preferentially capture broad H3K27me3 domains, whereas CUT&Tag provides sharper and more localized enrichment for both H3K27me3 and EZH2. Together, our results establish a practical framework for cross-platform epigenomic comparison and guide the selection of chromatin profiling strategies. [BMB Reports 2026; 59(4): 242-252]

INTRODUCTION

Recent advances in epigenomic technologies have greatly expanded our ability to profile chromatin landscapes, including histone post-translational modifications (PTMs) and chromatin-binding proteins (1-4). Among these various advances, chromatin immunoprecipitation sequencing (ChIP-seq) remains a foundational approach. Conventional ChIP-seq (convChIP) relies solely on formaldehyde crosslinking, which efficiently preserves protein–DNA interactions but can suffer from modest signal-to-noise ratio due to inefficient stabilization of protein-protein contacts (5). To overcome this limitation, double-crosslink ChIP-seq (dcChIP) protocols have been developed, incorporating both formaldehyde and disuccinimidyl glutarate (DSG) crosslinking (6). The double crosslink workflow enhances protein-chromatin stabilization by performing DSG-mediated protein-protein crosslinking prior to formaldehyde fixation, and hence yields sharper peaks in comparison to convChIP.

More recently, low-input chromatin profiling techniques such as CUT&RUN (CR) and CUT&Tag (CT) have transformed the field by enabling highly sensitive and high-resolution mapping from limited cell numbers (7, 8). CUT&RUN utilizes Protein A/G-MNase to target and cleave DNA near chromatin-bound proteins and performs particularly well for profiling chromatin-associated factors, typically requiring as input only 50,000-300,000 cells. CUT&Tag employs Protein A/G-Tn5 transposase to generate exceptionally high-resolution maps of histone PTMs and performs effectively with as few as 5,000-50,000 cells. Both techniques offer substantially improved signal-to-noise ratios and cleaner peak profiles relative to traditional ChIP-based methods, making them powerful tools for chromatin research, especially in low-input or rare cell populations (9).

The rapid adoption of these diverse chromatin profiling technologies has resulted in a growing number of publicly available epigenomic datasets generated using distinct experimental platforms. Direct comparison or integration of such datasets poses considerable challenge, as each method exhibits unique background characteristics, signal distributions, and dynamic ranges. Standard normalization approaches, such as counts-per-million (CPM) scaling, correct for sequencing depth but fail to account for assay-specific background structure, often leading to over- or underestimation of true biological signal. Alternative strategies, including exogenous spike-in normalization (10, 11), have been proposed to enable quantitative comparison across conditions, but their application is limited by experimental availability, batch effects, and incompatibility with many public datasets. These limitations underscore the need for a robust, biologically grounded normalization frame-

*Corresponding author. Tel: +82-2-740-8133; Fax: +82-2-740-7455; E-mail: chulhwan@snu.ac.kr
#These authors contributed equally to this work.

https://doi.org/10.5483/BMBRep.2025-0247

Received 31 December 2025, Revised 30 January 2026, Accepted 13 February 2026, Published online 30 April 2026

Keywords: ChIP-seq, CUT&RUN, CUT&Tag, Epigenomics, Polycomb

ISSN: 1976-670X (electronic edition)
© 2026 The Author(s).
This is an Open Access article distributed under the terms of the Creative Commons Attribution 4.0 International License (CC BY 4.0) (http://creativecommons.org/licenses/by/4.0/), which permits unrestricted use, distribution, and reproduction in any medium, provided the original work is properly cited.

work that enables cross-assay comparison without relying on external controls.

In the interest of enabling systematic comparison across platforms, we applied multiple chromatin profiling approaches to examine Polycomb Repressive Complex 2 (PRC2) and its associated repressive mark, H3K27me3, in the common setting of cardiomyocyte differentiation from human pluripotent stem cells (hPSCs). PRC2 maintains pluripotency in hPSCs by silencing lineage-specific genes and also reinforces cardiomyocyte identity during differentiation by repressing alternative lineage programs (12). This activity relies on an interplay among its core components, EZH1/2, EED, and SUZ12, which together establish and propagate H3K27me3 through a read-and-write mechanism (13-18). We specifically generated H3K27me3 datasets in cardiomyocytes using dcChIP, CUT&RUN, and CUT&Tag, and profiled EZH2 in hPSCs using dcChIP and CUT&RUN, and further complemented these data with matched public datasets. For comparisons, we implemented a locus-based normalization strategy in which genomic regions with stable PRC2 or H3K27me3 occupancy were used to derive assay-specific scaling factors. This approach enabled robust cross-assay alignment and revealed that all methods capture biologically relevant PRC2 domains while differing in signal-to-noise ratio and peak sharpness.

RESULTS

Polycomb target site-based normalization of H3K27me3 across chromatin profiling methods

To compare the genomic distribution of H3K27me3 across chromatin profiling techniques, we generated H3K27me3 datasets using dcChIP, CUT&RUN, and CUT&Tag; we also incorporated publicly available convChIP data (GSM2280006). To ensure biological consistency, all datasets correspond to the late stage of cardiomyocyte differentiation, the developmental time point at which hPSCs are differentiated into cardiomyocytes (Fig. 1A). As illustrated in Fig. 1B, convChIP utilizes formaldehyde crosslinking and sonication-based chromatin fragmentation, while dcChIP introduces a DSG crosslinking step prior to applying formaldehyde to better preserve protein–protein interactions. In CUT&RUN, an initial brief 0.1% formaldehyde crosslinking step stabilizes nuclear structure and improves nuclei isolation, after which protein A/G-MNase (pA/G-MNase) cleavage is performed. In contrast to the other methods, CUT&Tag is performed under native conditions, employing permeabilized nuclei and target-specific cleavage using protein A/G-Tn5 transposase (pA/G-Tn5). Sequencing quality metrics, including total read depth, mapping rates, and duplicate rates, are summarized in Table 1.

To visualize genome-wide H3K27me3 signal distribution, we initially normalized all datasets using CPM to correct for variation in sequencing depth (Fig. 1C). Visualization of genome browser tracks over a ~7 Mb region of chromosome 17, as well as canonical Polycomb targets such as the *HOXD* gene cluster and *NEUROD1* (19, 20), revealed substantial discrepancies in signal intensity across methods. Despite targeting the same histone modification in the same biological system (the late stage of cardiomyocyte differentiation), convChIP and dcChIP achieved middling signal intensity, CUT&RUN substantially attenuated signal, and CUT&Tag comparatively heightened enrichment at these loci (Fig. 1C). These discrepancies arise from intrinsic differences in background structure and signal distribution: CUT&RUN captures widespread low-level H3K27me3 across the genome, while CUT&Tag produces

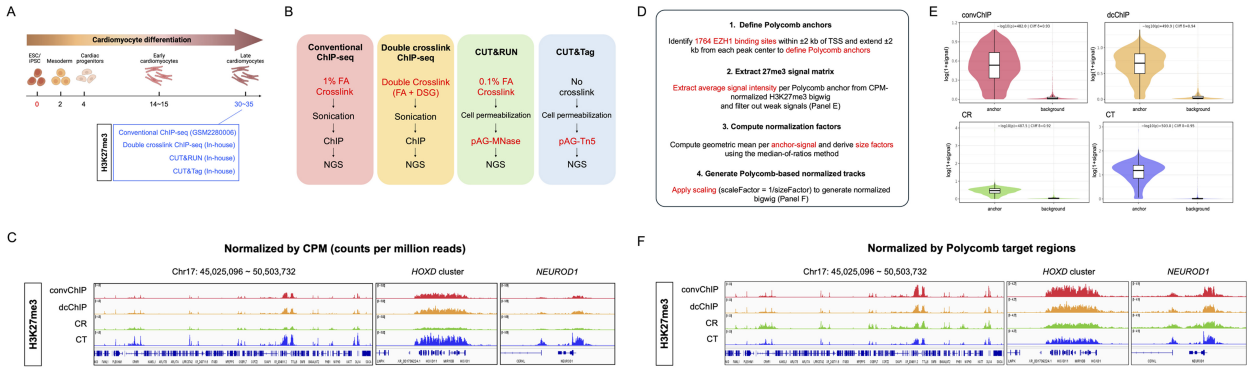


Fig. 1. Cross-assay normalization of H3K27me3 using Polycomb anchor regions. (A) Schematic representation of the differentiation model spanning from stage 1 hPSCs to stage 5 late cardiomyocytes and summary of the in-house and publicly available datasets used for cross-assay comparison of H3K27me3 in late cardiomyocytes. (B) Overview of the four chromatin profiling techniques compared, highlighting key steps and methodological features. (C) Raw genome browser tracks of H3K27me3 profiles generated by conventional ChIP-seq (red), double-crosslink ChIP-seq (orange), CUT&RUN (green), and CUT&Tag (blue). (D) Schema of the cross-assay normalization strategy applied to H3K27me3 datasets. (E) Violin plots showing log-scaled signal intensities at Polycomb anchor loci used for cross-assay normalization compared with background regions. Statistical differences between anchor and background were assessed using Wilcoxon rank-sum test, and effect sizes were computed using Cliff's delta. (F) Genome browser views of H3K27me3 signals following cross-assay normalization.

sharper focal peaks. This leads to underestimation or overestimation of signal intensity at true biological targets, especially for broadly distributed marks like H3K27me3. Such limitations of CPM normalization raise critical concerns for comparative epigenomic analysis across platforms.

To address this issue and ensure a fair cross-assay comparison, we developed a biologically informed normalization strategy based on Polycomb target regions, drawing conceptual inspiration from a prior study that identified invariant H3K27me3 regions by detecting windows of sustained high enrichment across conditions (Fig. 1D) (21, 22). While the previous study normalized H3K27me3 data using the invariant domains themselves, our strategy extends this concept to the cross-assay comparison by focusing on targets of a complementary Polycomb component, namely EZH1. We opted to use EZH1-defined targets because EZH1 is the predominant PRC2 catalytic form in late cardiomyocytes, whereas EZH2 is mainly expressed in proliferative cells (13-15).

We defined a robust set of Polycomb anchors by selecting 1,764 high-confidence EZH1 binding sites identified from EZH1 dcChIP-seq data in late cardiomyocytes (K-BDS: BioProject accession KAP241688), located within ±2 kb of transcription start sites (TSSs) and further extended ±2 kb from peak centers. To evaluate whether these anchors represent stable reference regions suitable for normalization, we compared H3K27me3 signal distributions at Polycomb anchor loci versus background genomic windows across all four assays using violin plots (Fig. 1E). Anchor regions consistently showed markedly higher signal intensities than background regions across all assays. Statistical testing further supported this distinction, with Wilcoxon rank-sum tests yielding low P-values as indicated. Effect size estimates were also substantial, with Cliff's delta values between 0.92 and 0.95, demonstrating that nearly all anchor regions exhibit stronger H3K27me3 signal than background. These results confirm that the selected Polycomb anchors represent stable and high-confidence reference regions suitable for cross-assay normalization.

For each method, average H3K27me3 signal intensity across these anchors was extracted from CPM-normalized bigwig files. Weak or non-specific signals were filtered out to minimize background influence. We then calculated anchor-wise geometric means and used the median-of-ratios method to derive size factors, which were applied to rescale each dataset. This normalization reduced method-dependent biases and allowed CUT&RUN and CUT&Tag signals at known Polycomb

Table 1. Summary of sequencing statistics for H3K27me3 and EZH2 profiling libraries

Condition	Assay	Replicates	Total reads (M)	Mapped (%)	Duplicates (%)
Stage 5 H3K27me3	convChIP	-	36.278712	98.59	7.1563
	dcChIP	-	16.967863	99.35	19.736
	CR	1	41.36823	99.46	1.8047
		2	44.899918	98.93	1.4768
	CT	1	26.408061	99.88	18.1234
		2	46.671073	99.87	27.0592
Stage 1 EZH2	convChIP	-	26.068259	98.2	17.5689
	dcChIP	1	44.589236	97.9	12.4297
		2	63.409692	98.91	8.9765
	CR	1	41.071252	98.08	3.893
		2	27.749586	96.62	8.9971
	CT	-	9.87633	97.37	44.2988

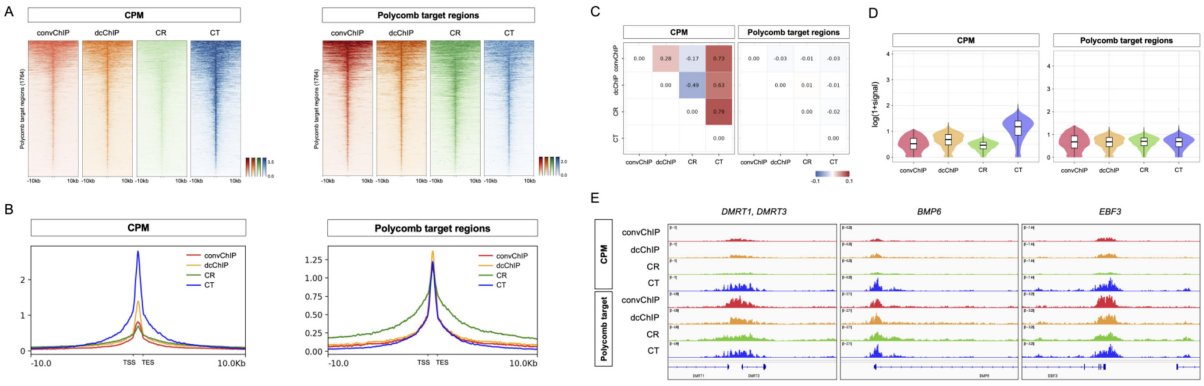


Fig. 2. Distinct H3K27me3 domain architectures revealed by ChIP-seq, CUT&RUN, and CUT&Tag. (A) Heatmaps displaying H3K27me3 signals normalized by counts per million (CPM) and signal in Polycomb target regions, with gene bodies rescaled to a uniform length and signals plotted relative to TSS and TES. Each row represents a 10 kb window. (B) Average signal intensity profiles derived from the four H3K27me3 mapping assays shown in A. (C) Pairwise effect size (Cliff's delta) heatmaps comparing H3K27me3 signal distributions across assays before (CPM) and after Polycomb target regions-based normalization. (D) Violin plots showing distributions of H3K27me3 signal intensity (log(1 + signal)) at Polycomb target regions across assays before and after normalization. Boxplots indicate median and interquartile ranges. (E) Genome browser views illustrating the respective peak patterns at selected genes.

targets to become comparable to ChIP-seq signals, enabling more accurate assessment of method-specific performance (Fig. 1F).

CUT&RUN captures broad H3K27me3 domains, while CUT&Tag resolves sharp peaks

To assess genome-scale H3K27me3 as perceived through different chromatin profiling techniques (convChIP, dcChIP, CUT&RUN, and CUT&Tag), we examined H3K27me3 signal distribution over 1,764 Polycomb target regions using both Polycomb target-based and CPM-normalized datasets. We visualized the normalized H3K27me3 signals using heatmaps (Fig. 2A) and average signal plots (Fig. 2B) centered on the defined Polycomb anchor regions (±10 kb). As discussed above, CPM normalization introduces biases that distort cross-assay comparisons: CUT&Tag showed sharp, high peaks, while CUT&RUN peaks appeared weaker and broader, and both convChIP and dcChIP exhibited diffuse signals (Fig. 2B, left). This again emphasizes the need for Polycomb-target-based normalization to correct for such discrepancies.

To validate Polycomb target-based normalization, we quantified pairwise differences in anchor signal distributions using Cliff's delta (Fig. 2C). Substantial method-dependent differences were observed prior to normalization, whereas all pairwise Cliff's delta values converged toward zero afterward, indicating effective equalization of anchor signal distributions. Violin plots similarly showed marked pre-normalization differences that became highly aligned following normalization (Fig. 2D).

With method-specific scaling biases effectively removed, Polycomb target-based normalization enabled a fair comparison of signal shape and localization. Specifically, CUT&RUN retained a broad distribution of H3K27me3 around the anchors compared to other methods, consistent with its higher sensitivity to widely distributed chromatin domains (Fig. 2B, right, green line). CUT&Tag likewise continued to show less background signal compared to other methods, suggesting enhanced resolution (Fig. 2B, right, blue line).

Together, these results indicate that while normalization corrects for total signal discrepancies, each method retains an intrinsic signal architecture that reflects the unique biochemical mechanisms it leverages (Fig. 2B, E). CUT&RUN appears to capture broader chromatin states, whereas CUT&Tag delivers sharper positional resolution—features that should be considered when selecting a profiling strategy for specific biological questions.

H3K27me3-invariant-promoter-based normalization enables cross-method comparison of EZH2 signal

Following our analysis of H3K27me3 in hPSC-derived late cardiomyocytes, we next focused on comparing the genomic distribution of EZH2, the catalytic subunit of PRC2, as determined by multiple chromatin profiling techniques in hPSCs. PRC2 containing EZH2 (PRC2/EZH2) is responsible for depositing H3K27me3, making its localization a critical readout of PRC2 activity and an essential complement to the histone modification itself (13, 15, 16). For this analysis, we profiled EZH2 signal using dcChIP and CUT&RUN and incorporated publicly available convChIP (ENCSR045YHA) and CUT&Tag (GSM8352703) data (Fig. 3A, B). All datasets were derived from the human pluripotent stem cells, with CUT&Tag data generated in hESCs and the remaining assays performed in hiPSCs, thereby maintaining a broadly consistent pluripotent cellular background for comparative analysis (23). Notably, Polycomb-associated chromatin features are known to be highly conserved between hESCs and hiPSCs, supporting cross-

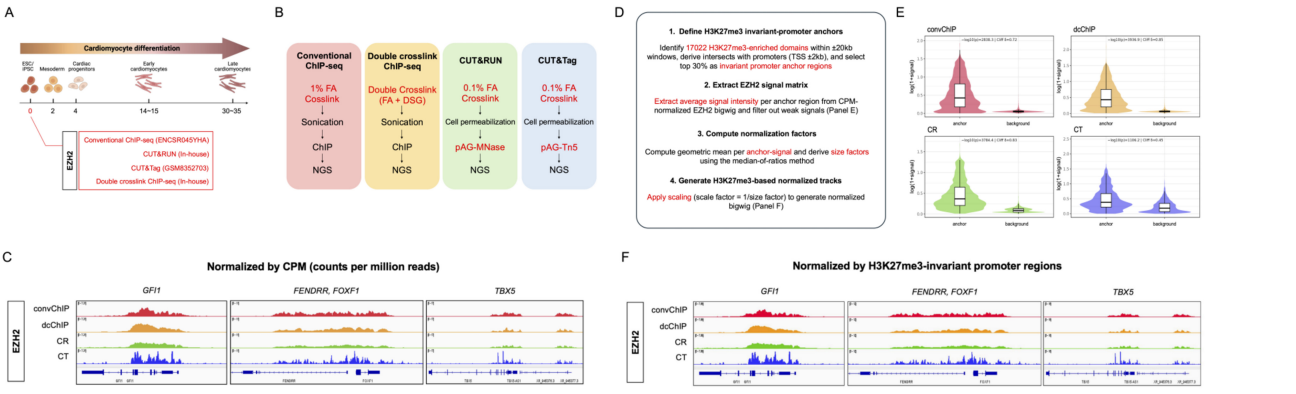


Fig. 3. H3K27me3-invariant promoters provide a reference framework for EZH2 signal normalization. (A) Schematic representation of the differentiation model spanning from stage 1 hPSCs to stage 5 late cardiomyocytes and summary of the in-house and publicly available datasets used for cross-assay comparison of EZH2 in stage 1 hPSCs. (B) Overview of the four chromatin profiling techniques for EZH2, highlighting key steps and methodological features. (C) Raw genome browser tracks of EZH2 profiles generated by conventional ChIP-seq (red), double-crosslink ChIP-seq (yellow), CUT&RUN (green), and CUT&Tag (blue). (D) Schema of the cross-assay normalization strategy applied to EZH2 datasets. (E) Violin plots showing log-scaled signal intensities at H3K27me3-invariant-promoter anchors, genomic loci used for cross-assay normalization compared with background regions. Statistical differences between anchor and background were assessed using Wilcoxon rank-sum test, and effect sizes were computed using Cliff's delta. (F) Genome browser views of EZH2 signals following cross-assay normalization.

assay comparison focused on relative signal architecture rather than absolute signal levels (24). The corresponding sequencing quality metrics for these datasets are provided in Table 1.

When using CPM normalization, EZH2 signals from all examined chromatin profiling methods are enriched at Polycomb target sites, suggesting relative consistency (Fig. 3C). To confirm whether CPM-based normalization is sufficient for comparisons, we developed an alternative normalization strategy based on H3K27me3-enriched promoter regions (Fig. 3D). Specifically, we identified 17,022 broad H3K27me3 domains associated with promoter regions (±2 kb), calculated the average H3K27me3 signal for each region across replicates. From these, the top 30% most stable regions were selected as anchor loci, as this threshold maintained stable scaling factor relationships while avoiding both over-stringency and excessive inclusion of low-signal promoters.

To assess whether these H3K27me3-invariant promoter anchor regions represent stable reference loci, we compared EZH2 signal distributions at the anchor regions and background windows across all four assays using violin plots (Fig. 3E). Anchor regions displayed significantly higher signal intensities than background regions in every dataset, and Wilcoxon rank-sum tests yielded low P-values as indicated. Effect size estimates, however, varied across methods: ConvChIP, dcChIP, and CUT&RUN all showed large effect sizes, reflecting strong enrichment of EZH2 at invariant promoters; in contrast, CUT&Tag showed a more modest effect size. This attenuation is consistent with contextual factors; namely, CUT&Tag is generally optimized for histone PTM profiling rather than chromatin-associated proteins (9). Although native or low-salt conditions have been reported to partially mitigate protein loss, an inherent trade-off remains, as the method's high specificity and low background can come at the expense of sensitivity for PRC2 components (8, 9). Together, these considerations explain the reduced effect size observed for CUT&Tag while still supporting the overall validity of invariant promoters as suitable reference regions for EZH2 normalization.

We then extracted average EZH2 signal intensities across these anchors from CPM-normalized datasets, filtered out low-signal regions, and calculated size factors using the median-of-ratios method. These were used to generate scaled bigwig tracks, allowing for signal normalization across profiling platforms. Representative genome browser views demonstrated the effectiveness of this normalization approach (Fig. 3F). CUT&Tag produced sharp and discrete EZH2 peaks tightly localized to promoter regions, whereas CUT&RUN, dcChIP, and convChIP showed moderate enrichment with more diffuse peak shapes.

CUT&Tag emphasizes sharp, promoter-confined EZH2 enrichment compared to other methods

To investigate how chromatin profiling methods differ in the detection of EZH2, we examined genome-scale signal distribution over 17,022 invariant promoter anchors, using both CPM and anchor-based normalization approaches. Heatmaps and average signal plots were generated to compare convChIP, dcChIP, CUT&RUN, and CUT&Tag profiles (Fig. 4A, B).

In CPM-normalized datasets, EZH2 signals from all methods were enriched at Polycomb target sites, and inter-method differences were already modest compared to the pronounced variation observed for H3K27me3 (Figs 2B, left; 4B, left), consistent with the intrinsically narrow, promoter-confined binding profile of EZH2. Anchor-based normalization using H3K27me3-invariant promoter regions further reduced these residual differences, yielding more directly comparable EZH2

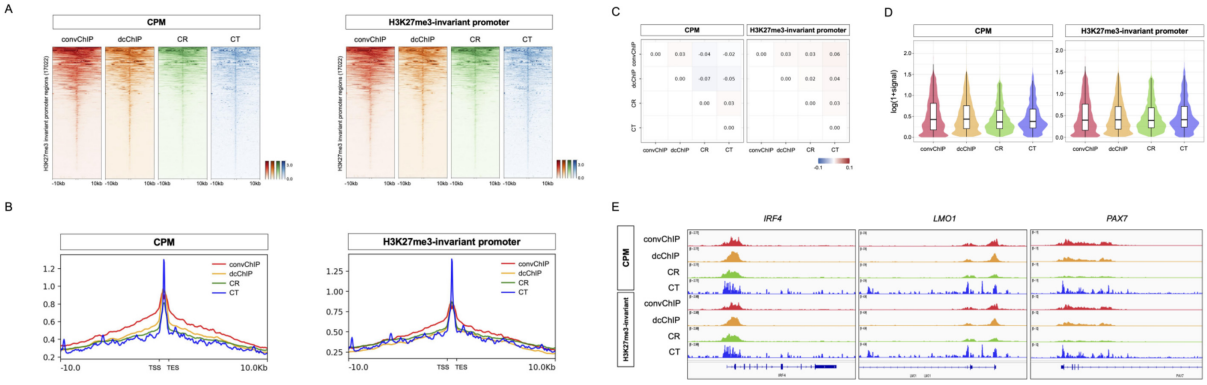


Fig. 4. Method-dependent differences in EZH2 peak localization and resolution. (A) Heatmaps of EZH2 signals normalized by CPM and by signal in H3K27me3-invariant anchor loci, with gene bodies rescaled to a uniform length and signals plotted relative to TSS and TES. Each row represents a 10 kb window. (B) Average signal intensity profiles derived from the four EZH2 mapping assays shown in A. (C) Pairwise effect size (Cliff's delta) heatmaps comparing EZH2 signal distributions across assays before (CPM) and after H3K27me3-invariant promoter regions-based normalization. (D) Violin plots showing distributions of EZH2 signal intensity (log(1 + signal)) at H3K27me3-invariant promoter regions across assays before and after normalization. Boxplots indicate median and interquartile ranges. (E) Genome browser views illustrating the respective peak patterns at selected genes.

profiles across methods (Fig. 4B, right).

Quantification using Cliff's delta confirmed that pairwise differences were small even prior to normalization and remained near zero afterward, with no introduction of method-specific biases (Fig. 4C). Violin plots of EZH2 signal distributions at invariant promoter anchors similarly demonstrated improved alignment of medians and central distributions following normalization (Fig. 4D).

After normalization, CUT&Tag exhibited highly localized, sharply peaked EZH2 enrichment concentrated at TSSs, reflecting the focal integration properties of Tn5-mediated profiling (Fig. 4B, E). A spiky peripheral signal was also observed, likely arising from the discrete, event-based nature of CUT&Tag (8).

Cross-assay coherence in Polycomb-regulated gene sets and divergent signal resolution across profiling methods

To evaluate whether cross-assay normalization preserved the expected Polycomb targeting characteristics, we performed Gene Ontology enrichment analysis on the union of genes containing promoter-proximal peaks (TSS ± 3 kb) across the four profiling methods. For both H3K27me3 in late cardiomyocytes and EZH2 in hPSCs, the top enriched terms were dominated by developmental and pattern-specification processes, including regulators of tissue identity and lineage commitment (Fig. 5A, B). These results confirm that, despite methodological differences, all four assays consistently capture Polycomb-associated repression programs linked to embryonic patterning and differentiation control.

Next, to assess method-specific differences in signal-to-noise and peak sharpness, we jointly computed FRiP (fraction of reads in peaks) values and the inverse of FWHM (full width at half maximum) (25-27). For H3K27me3 in late cardiomyocytes, CUT&Tag produced the highest FRiP values and the narrowest peaks, reflecting both superior signal-to-noise performance and the sharpest positional resolution (Fig. 5C). dcChIP showed an increase in FRiP relative to convChIP, accompanied by a modest improvement in peak. Whereas CUT&RUN exhibited the lowest FRiP and sharpness values, this reflects its preferential capture of broad H3K27me3 domains. For EZH2 in hPSCs, CUT&Tag again produced by far the sharpest peaks and maintained a high FRiP, consistent with its strong performance for high-resolution profiling (Fig. 5D). CUT&RUN provided intermediate performance in FRiP value and peak sharpness, whereas convChIP and dcChIP displayed lower FRiP and broader EZH2 profiles, with dcChIP showing the lowest values for both metrics. Because EZH2 binding is promoter-centered and intrinsically narrow in signal, both FRiP and 1/FWHM values were substantially smaller than for the broader H3K27me3 domains (Fig. 5C, D) (28).

Consistent with these quantitative metrics, delta heatmaps provided spatial evidence for method-dependent differences in signal distribution. For H3K27me3 in late cardiomyocytes, the △(conv−dc) comparison revealed that dcChIP exhibits relatively higher enrichment at peak centers compared to convChIP, whereas convChIP displays more diffuse signal distribution in a subset of regions (Fig. 5E, left). In contrast, the △(CR−CT) comparison demonstrated CUT&Tag to generate sharper and more focused peak summits, while CUT&RUN captures broader

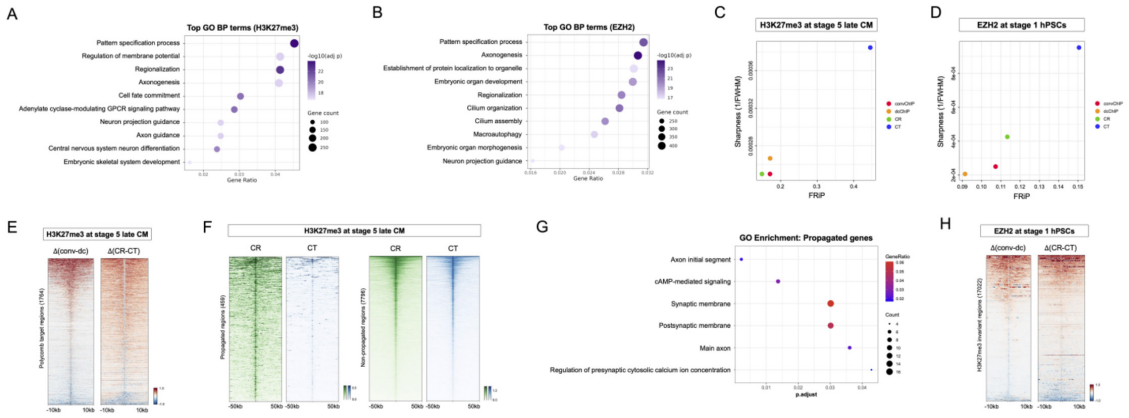


Fig. 5. Consistent Polycomb target gene identification across assays with divergent signal properties. (A, B) Top 10 Gene Ontology Biological Process (GO BP) terms enriched among the union of genes detected by all methods, profiling H3K27me3 in stage 5 cardiomyocytes (A) and EZH2 in stage 1 hPSCs (B). (C, D) Scatter plots illustrating signal-to-noise and peak sharpness characteristics for each method, profiling H3K27me3 (C) and EZH2 (D). The x-axis indicates FRiP (signal-to-noise), and the y-axis shows peak sharpness (1/FWHM). (E) Delta heatmaps showing △(conv−dc) and △(CR−CT) for H3K27me3 at Polycomb anchor regions in stage 5 cardiomyocyte. Each row represents a 10 kb window centered on anchor regions, scaled to uniform length. (F) Heatmaps of propagated (left) and non-propagated (right) H3K27me3 regions in CR and CT samples. Signals were normalized using Polycomb target regions, and each row was centered on H3K27me3 nucleation sites. Propagated regions were defined using DESeq2 ($|\log2FC| > 1$ and P-value < 0.05). Each row represents a 50 kb window. (G) GO terms of genes located near H3K27me3 propagated regions. (H) Delta heatmaps showing △(conv−dc) and △(CR−CT) for EZH2 in stage 1 hPSCs. Each row represents a 10 kb window centered on invariant promoter regions.

flanking domains across majority fo Polycomb anchor regions (Fig. 5E, right). Distinct from the other delta heatmaps, the △(CR–CT) analysis particularly highlighted the broad H3K27me3 signal pattern across Polycomb target regions in CUT&RUN, consistent with the broader domain-capture characteristics observed in earlier analyses (Figs. 2B, E and 5E, right).

To determine whether this broadened pattern reflects biologically meaningful domain propagation rather than a global assay-intrinsic bias, we classified 8,255 H3K27me3 nucleation sites into propagated and non-propagated regions based on EZH1-defined anchors (Fig. 5F). CUT&RUN selectively amplified signal within propagated regions, while non-propagated regions showed comparable profiles across methods (Fig. 5F). Genes associated with propagated domains were enriched for non-cardiac lineage programs, supporting biologically coherent Polycomb-mediated repression (Fig. 5G).

In contrast, for EZH2 in hPSCs, delta heatmaps revealed method-dependent differences confined to a relatively narrow spatial range (Fig. 5H). While dcChIP showed slightly stronger enrichment at peak centers than convChIP, and CUT&Tag produced sharper central peaks relative to CUT&RUN, no domain-scale expansion across the majority of peaks analogous to the H3K27me3 propagation pattern was observed. These findings indicate that inter-method differences for EZH2 primarily reflect resolution and peak sharpness rather than differential representation of broad chromatin domains.

DISCUSSION

In this study, we systematically compared four chromatin profiling methods (convChIP-seq, dcChIP-seq, CUT&RUN, and CUT&Tag) across two biologically coherent contexts: H3K27me3 in late human cardiomyocytes and EZH2 mapping in human pluripotent stem cells. By integrating in-house and public datasets and developing biologically informed normalization strategies, we assessed the relative strengths, limitations, and characteristic signal architectures of the four assays. Our findings highlight several principles that should guide the selection and interpretation of chromatin profiling methods, especially for broad histone modifications such as H3K27me3 and sharply localized chromatin-bound proteins such as EZH2.

Cross-assay comparison is enabled by biologically informed normalization

The increasing availability of public epigenomic datasets has made it common to compare data generated using different sequencing platforms and fundamentally distinct biochemical workflows (4), rendering normalization a major challenge in cross-assay analyses. Standard CPM normalization fails to account for platform-specific background architecture, often leading to overestimation (CUT&Tag) or underestimation (CUT&RUN) of signal amplitude at *bona fide* Polycomb domains. Moreover, widely used spike-in strategies cannot be uniformly applied across heterogeneous profiling methods, limiting their utility for cross-platform comparisons (11).

By implementing normalization based on biologically invariant regions, EZH1-bound Polycomb anchors for H3K27me3 and H3K27me3-enriched promoters for EZH2, we were able to harmonize signal scales without distorting intrinsic signal shapes. This strategy allowed direct comparison of signal architecture and resolution across methods, providing a more accurate view of each technique's performance than depth-based normalization alone.

Although hESCs and hiPSCs exhibit context-dependent epigenetic differences, primarily attributable to reprogramming history, Polycomb-associated chromatin features are relatively conserved between these pluripotent cell type (24). By anchoring normalization to invariant Polycomb features rather than global signal depth, our approach facilitates method-focused comparison of signal architecture while minimizing confounding effects attributable to cell line origin.

CUT&RUN captures broad and propagated chromatin states

Across analyses, CUT&RUN consistently exhibited broader H3K27me3 distribution surrounding Polycomb anchors compared with other methods. Importantly, our propagated-region analysis demonstrates that this broadened signal is selectively enriched at biologically defined propagation sites. Genes associated with these domains are enriched for non-cardiac lineage programs, supporting functional Polycomb-mediated repression. These findings indicate that the broadened pattern detected by CUT&RUN reflects coherent domain-level representation rather than a simple assay artifact. Mechanistically, this may arise from heightened sensitivity to peripheral H3K27 methylation states and/or intrinsic MNase cleavage properties. Regardless of the precise mechanism, CUT&RUN appears particularly well suited for mapping diffuse histone modifications and extended repressive domains.

CUT&Tag offers superior peak precision but may undersample peripheral occupancy

In contrast to CUT&RUN, CUT&Tag generated exceptionally sharp and focal peaks for both H3K27me3 and EZH2, especially after normalization. For H3K27me3, CUT&Tag detected strong summit-enriched peaks embedded within Polycomb domains. For EZH2, the method displayed nearly ideal promoter-confined peaks, consistent with the tight recruitment of PRC2 to CpG-rich promoter regions in hPSCs (29). However, because Tn5-mediated tagmentation favors accessible chromatin, CUT&Tag may undersample weak or peripheral enrichment within broad domains (30). Thus, CUT&Tag excels at positional precision, whereas CUT&RUN better captures domain-scale architecture.

Generalizability of biologically informed normalization frameworks

Although the normalization strategies presented this paper were developed in the context of Polycomb-associated features,

the underlying principle is broadly applicable to other chromatin profiling targets. The core concept relies on identifying biologically invariant or stable reference regions that can serve as internal anchors for signal scaling across assays (10). For histone modifications with distinct genomic distributions, such as H3K4me3, anchor regions could be defined based on stably marked promoters or transcription start sites shared across conditions (21). Similarly, for other chromatin binding proteins, normalization anchors may be derived from constitutively occupied binding sites. Importantly, the choice of anchor regions must be customized to the biological properties (25). Thus, while the normalization framework provides a generalizable strategy for cross-assay comparison, its successful application depends on careful, target-specific definition.

Implications for studying PRC2 biology and chromatin repression

Our analysis has direct implications for Polycomb biology (15-18, 31-35). PRC2-mediated repression relies on both sharply localized catalytic activity at promoters and broad propagation of H3K27me3 across distal genomic regions. The combination of CUT&Tag and CUT&RUN therefore provides a complementary view: CUT&Tag pinpoints the core catalytic footprint of PRC2, whereas CUT&RUN reveals the epigenetic landscape shaped by its spreading activities. This dual perspective may be particularly informative for understanding developmental transitions, lineage specification, and pathological states such as cancer or abnormal PRC2 activation (36-38).

Overall, our cross-assay comparison demonstrates that while all four methods can capture biologically meaningful PRC2 and H3K27me3 patterns, their performance varies considerably depending on the genomic architecture (39). CUT&RUN excels at depicting domain-wide repressive landscapes, CUT&Tag provides unmatched precision at peak summits, and ChIP-based methods offer stable intermediate profiles. Our normalization strategies reveal that these differences reflect method-intrinsic properties rather than biological inconsistencies. Together, these findings offer a practical framework for choosing appropriate profiling tools and interpreting chromatin datasets and also provide new insights into how Polycomb-mediated repression is represented across mapping modalities.

Limitations of the study

Biologically informed normalization enables integration of datasets generated using different experimental protocols; however, several limitations should be noted. Although hiPSCs and hESCs share broadly similar epigenetic landscapes, subtle differences in cell origin or reprogramming history may introduce regional variability not fully captured by normalization. In addition, datasets generated across laboratories may differ in experimental parameters, including starting material, washing conditions, or crosslinking strategies. While our analyses demonstrate overall global comparability, localized differences at specific genomic regions cannot be entirely excluded. Validation using matched samples from identical cellular backgrounds would further strengthen future locus-specific investigations.

MATERIALS AND METHODS

Human induced pluripotent stem cells (hiPSC) culture and cardiomyocyte differentiation

hiPSCs (CAL-hiPSC-8) cell line was cultured using the StemMACS (Miltenyi Biotec, 130-104-368) medium in Matrigel (Corning, 354234)-coated cell culture dishes. 10 μM Y-27632 (Tocris, 1254) was added for the first 24 h after passage. The medium was changed daily, and hiPSCs were allowed to grow in StemMACS for 3 days until the cells were 80-100% confluent. At day 0, cells were treated with 6 μM/ml CHIR99021 (Tocris, 4423) in Media #1 (RPMI1640 (ThermoFisher Scientific, 11875 093)/B-27 minus insulin (ThermoFisher Scientific, A1895601)/ Penicilin-Streptomycin (ThermoFisher Scientific, 15140-122)). After 24 h, the medium was changed to Media #1 supplemented with 6 μM/ml CHIR99021. At day 2, the medium was changed to Media #1 supplemented with 2 μM/ml C59 (Wnt inhibitor/Tocris, 5148). After 24 h, the medium was changed to Media #1 supplemented with 2 μM/ml C59. At day 4, the medium was replaced with Media #1 and freshly changed after 24 h. At day 6, the medium was replaced with Media #2 (RPMI1640/B-27 (ThermoFisher Scientific, 17504044)/Penicilin-Streptomycin) and freshly changed every 2 days. Contracting cells began to appear at day 7 to day 10. From day 10 to day 13, the medium was replaced with Purification media (RPMI1640 without glucose (ThermoFisher Scientific, 11879020)/ B-27 (ThermoFisher Scientific, 17504044)/Penicilin-Streptomycin/ L-lactic acid (Sigma, L4263)) to metabolically select and purify cardiomyocytes (hiPSC-CMs). After purification of cardiomyocytes, the medium was replaced with Media #2. At day 15, cardiomyocytes were detached using 0.25% trypsin-EDTA (ThermoFisher Scientific, 25200072) to seed onto Matrigel-coated cell culture dish supplemented with Media #2. At day 18, the medium was replaced with Media #2 and freshly changed every 2 days.

Double-crosslink ChIP-seq

A double-crosslink ChIP-seq experiment was conducted as previously reported (40). Briefly, 5×10^6 cardiomyocytes or hiPSCs were first double crosslinked using 2 mM DSG for 35 minutes, followed by 1% formaldehyde for an additional 10 minutes. Nuclei were subsequently isolated, and the chromatin was lysed using 1% SDS buffer. The lysate was sonicated with a Covaris S220 (175 peak incident power, 10% duty factor, 200 cycles/burst) for 430 seconds to yield soluble chromatin. The resulting chromatin was incubated overnight at 4^oC with primary antibodies (EZH1 (Proteintech, 20852-1-AP), EZH2 (CST, 5246), H3K27me3 (CST, 9733)) conjugated to Dynabeads Protein A. Following sequential washes with Buffers A, B, and C, the chromatin was reverse crosslinked

overnight at 65°C after 37°C RNase treatment. The resulting DNA fragments of about 200 bp were purified using AMPure XP beads, and sequencing libraries were prepared with the NEB DNA library prep kit and sequenced on an Illumina NovaSeq 6000 platform (100 bp paired-end mode).

CUT&RUN

A CUT&RUN was carried out according to the manufacturer's protocol (Epicypher). Briefly, cells were mildly crosslinked by 0.1% formaldehyde for 1 min, and nuclei were isolated. Subsequently, nuclei were immobilized on activated ConA–coated magnetic beads. The bead-bound samples were permeabilized in digitonin-containing buffer and incubated with a target-specific primary antibody overnight at 4°C, followed by a short incubation with a secondary antibody. After washing, pAG-MNase was added to bind antibody–chromatin complexes. Targeted chromatin cleavage was initiated by calcium activation at 4°C and released DNA fragments were collected in the supernatant following MNase digestion and stop buffer treatment. The CUT&RUN-enriched DNA was purified and quantified, and sequencing libraries were generated using the NEB DNA library Prep Kit. Final libraries were sequenced on an MGI DNBSEQ-G400 platform (100 bp paired-end mode).

CUT&Tag

A CUT&Tag was also carried out according to the manufacturer's protocol (Epicypher). Briefly, nuclei were isolated using Nuclear Extraction Buffer (20 mM HEPES-NaCl (pH 7.9), 10 mM KCl, 0.1% Triton X-100, 20% Glycerol, 0.5 mM Spermidine, and protease inhibitors). The isolated nuclei were immobilized on ConA-coated magnetic beads (Epicypher, 21-1401). The bead-bound nuclei were then incubated overnight at 4°C on a nutator with 0.5 μg of H3K27me3 primary antibody (CST, 9733). The complexes were subsequently incubated with a secondary antibody for 30 minutes at room temperature. After washing, pAG-Tn5 transposase (Epicypher, 15-1017) was added and incubated for 1 hour at room temperature to facilitate binding. The target DNA was tagmented by incubating the washed complexes for 1 hour at 37°C in the presence of 10 mM MgCl2.Tagmented DNA was released from the complexes using SDS release buffer and amplified via non-hot start PCR using 2x PCR master mix (Epicypher, 15-1018) and corresponding i5/i7 barcoded primers. Libraries were purified using AMPure XP beads (Beckman, A63881) and sequenced in 100 bp paired-end mode on an Illumina NovaSeq 6000 platform (100 bp paired-end mode).

Data pre-processing

For the stage 5 (stg5) H3K27me3 analysis, the dataset comprised one publicly available conventional ChIP-seq dataset, one in-house double-crosslink ChIP-seq dataset, two independent in-house CUT&RUN datasets, and two independent in-house CUT&Tag datasets. For the stage 1 (stg1) EZH2 analysis, the dataset included one publicly available conventional ChIP-seq dataset, two independent in-house double-crosslink ChIP-seq datasets, two independent in-house CUT&RUN datasets, and one publicly available CUT&Tag dataset.

For public datasets, raw sequencing data were downloaded from the SRA using prefetch and fasterq-dump (GEO accessions: GSM2280006, GSM8352703) or directly downloaded from the ENCODE portal (ENCODE experiment accession: ENCSR045YHA). For all datasets, reads were aligned to the hg38 genome with BWA-MEM (v0.7.17). PCR duplicate reads were marked using the MarkDuplicates function in Picard, and low-quality reads (MAPQ $<$ 10) were removed. Peak calling was performed with MACS2, using narrow-peak mode for EZH2/EZH1 and broad-peak mode for H3K27me3 ($q = 0.01$). Coverage tracks were generated with bamCoverage, firstly using CPM normalization, a minimum mapping quality of 30, and exclusion of duplicate-marked reads. These CPM-normalized bigwig files were used for genome browser visualization, heatmaps, and average profiles.

Cross-assay normalization and QC

To compare H3K27me3 and EZH2 profiles across convChIP-seq, dcChIP-seq, CUT&RUN, and CUT&Tag, we applied normalization strategy based on biologically stable anchor regions.

For H3K27me3 normalization in late cardiomyocytes, PRC2 anchor loci were defined as promoter regions (TSS $\pm$ 2 kb) overlapping EZH1 peaks, with fixed 4-kb windows centered on peak summits. Mean signals from CPM-normalized bigwig files were calculated for each anchor region, and low-signal anchors, and low-signal anchors below ~40% of the global median signal were excluded. Assay-specific size factors were computed using a median-of-ratios approach relative to the geometric mean across assays, and reciprocal values were applied to generate scaled bigwig files.

For EZH2 normalization in hPSCs, we used a complementary approach based on H3K27me3-invariant promoters identified from CUT&Tag data. Genome-wide 20-kb windows were ranked by H3K27me3 enrichment, and the top 10% were intersected with promoter regions (TSS $\pm$ 2 kb) to define invariant H3K27me3 promoters (22). From these, the top 30% most stable regions were selected as anchor loci. As above, mean EZH2 signal was calculated within each anchor region, low-signal anchors below ~40% of the global median signal were filtered, and assay-specific scaling factor were computed using the same median-of-ratios framework.

Anchor suitability was assessed by comparing signal distributions at anchor loci versus background regions using log-transformed values, Wilcoxon rank-sum tests, and Cliff's delta.

Analysis

To statistically validate normalization performance, pairwise differences in signal distributions across profiling methods were quantified using Cliff's delta, a non-parametric effect size measure. Cliff's delta values were computed for anchor-region signal distributions before and after normalization. In addition,

signal distributions were visualized using violin plots to compare changes in central tendency and distributional spread across methods. All statistical analyses and visualizations were performed in R.

Peak-based gene sets for downstream analyses were generated from the cross-assay normalized datasets. For each assay, MACS2 peak calling was performed on the normalized BAM files, and peaks overlapping promoter regions (defined as ± 3 kb from the transcription start site) were annotated to their corresponding genes using Python-based processing scripts. Gene Ontology (GO) enrichment analyses were carried out using the clusterProfiler package in R, using the union gene sets as input.

To evaluate assay performance, FRiP (fraction of reads in peaks) scores were calculated from the normalized BAM files and their respective peak BED files. Peak sharpness was quantified as the inverse of the full width at half maximum (1/FWHM), where FWHM values were computed from matrices generated by deepTools computeMatrix and subsequently processed in R. Scatter plots integrating FRiP and 1/FWHM were generated using R to compare the signal quality across profiling methods.

Delta heatmaps were generated using bigwigCompare with the subtract operation. The resulting delta bigwigs were processed with deepTools computeMatrix. Heatmaps and averaged profiles were visualized using plotHeatmap and plotProfile.

Data availability

Newly generated datasets have been deposited in GEO (GSE314247), and previously generated datasets are available in the Korea BioData Station (BioProject KAP241688). Additional information required for reanalysis is available from the lead contact upon request. Custom data processing and analysis scripts are available at GitHub (https://github.com/amyoh999-dev/ChIPs-cross-assay-normalization-).

ACKNOWLEDGEMENTS

We thank members of the Lee laboratory for valuable discussions. This work was supported by the Korean government (MSIT) (NRF2021R1C1C1013220, RS-2022-NR070833, RS-2023-00223069, RS-2023-00211612, RS-2025024523684, RS-2025-02217909), the BK21 Four Biomedical Science Program, and the SNUH Kun-hee Lee Child Cancer and Rare Disease Project Foundation (22B-001-0100). Additional support was provided by the Research Resettlement Fund for New Faculty at SNU, the Creative-Pioneering Researchers Program (SNU), the SNUBH–SNU Medicine Collaborative Research Fund (16-2026-0001), SNU Research Grant for Interdisciplinary Collaboration (550-20250081), the AI-Bio Research Grant (SNU), the Doosan Yonkang Foundation (SNUH-30-2024-0440), and NAVER (SNUH-3720242170). Figures were created with BioRender.com.

AUTHORS' CONTRIBUTION

Y-J.O., H-B.K. and C-H.L. conceptualized and designed the study. Y-J.O. and H-B.K. in C-H.L. lab, S.L. in I.J. lab, S.P. and Y-G.P. in S-H.M. lab conducted the experiments and bioinformatics analyses. Y-J.O., H-B.K. and C-H.L. wrote the manuscript.

CONFLICTS OF INTEREST

The authors have no conflicting interests.

REFERENCES

1. Zang C, Schones DE, Zeng C, Cui K, Zhao K and Peng W (2009) A clustering approach for identification of enriched domains from histone modification ChIP-Seq data. Bioinformatics 25, 1952-1958
2. Skene PJ and Henikoff S (2015) A simple method for generating high-resolution maps of genome-wide protein binding. eLife 4, e09225
3. Meers MP, Bryson TD, Henikoff JG and Henikoff S (2019) Improved CUT&RUN chromatin profiling tools. eLife 8, e46314
4. Mehrmohamadi M, Sepehri MH, Nazer Na and Norouzi MR (2021) A comparative overview of epigenomic profiling methods. Front Cell Dev Biol 9, 714687
5. Hoffman EA, Frey BL, Smith LM and Auble DT (2015) Formaldehyde crosslinking: a tool for the study of chromatin complexes. J Biol Chem 290, 26404-26411
6. Bao Y, Cacioppo R, Crisp A et al (2025) Protocol for double-crosslinking ChIP-seq to improve data quality and enhance detection of challenging chromatin targets. STAR Protoc 6,104171
7. Skene PJ and Henikoff S (2017) An efficient targeted nuclease strategy for high-resolution mapping of DNA binding sites. eLife 6, e21856
8. Kaya-Okur HS, Wu SJ, Codomo CA et al (2019) CUT&Tag for efficient epigenomic profiling of small samples and single cells. Nat Commun 10, 1930
9. Kaya-Okur HS, Janssens DH, Henikoff JG, Ahmad K and Henikoff S (2020) Efficient low-cost chromatin profiling with CUT&Tag. Nat Protoc 15, 3264-3283
10. Egan B, Yuan CC, Craske ML et al (2016) An Alternative approach to ChIP-Seq normalization enables detection of genome-wide changes in histone H3 lysine 27 trimethylation upon EZH2 inhibition. PLoS One 11, e0166438
11. Orlando DA, Chen MW, Brown VE et al (2014) Quantitative ChIP-Seq normalization reveals global modulation of the epigenome. Cell Rep 9, 1163-1170
12. Kook H, Seo S-B and Jain R (2017) EZ Switch From EZH2 to EZH1. Circ Res 121, 91-94
13. Yu JR, Lee CH, Oksuz O, Stafford JM and Reinberg D (2019) PRC2 is high maintenance. Genes Dev 33, 903-935
14. Lee SH, Li Y, Kim H, Eum S, Park K and Lee CH (2022) The role of EZH1 and EZH2 in development and cancer. BMB Rep 55, 595-601

15. Lee CH, Holder M, Grau D et al (2018) Distinct stimulatory mechanisms regulate the catalytic activity of polycomb repressive complex 2. Mol Cell 70, 435-448.e5
16. Lee CH, Yu JR, Kumar S et al (2018) Allosteric activation dictates PRC2 activity independent of its recruitment to chromatin. Mol Cell 70, 422-434.e6
17. Popoca L and Lee CH (2022) Techniques to study automethylation of histone methyltransferases and its functional impact. Methods Mol Biol 2529,109-120
18. Lee CH, Yu JR, Granat J et al (2019) Automethylation of PRC2 promotes H3K27 methylation and is impaired in H3K27M pediatric glioma. Genes Dev 33, 1428-1440
19. Fourkala E-O, Hauser-Kronberger C, Apostolidou S et al (2010) DNA methylation of polycomb group target genes in cores taken from breast cancer centre and periphery. Breast Cancer Res Treat 120, 345-355
20. Woo CJ, Kharchenko PV, Daheron L, Park PJ and Kingston RE (2010) A region of the human HOXD cluster that confers polycomb-group responsiveness. Cell 140, 99-110
21. Adriaens ME, Prickaerts P, Chan-Seng-Yue M et al (2016) Quantitative analysis of ChIP-seq data uncovers dynamic and sustained H3K4me3 and H3K27me3 modulation in cancer cells under hypoxia. Epigenetics Chromatin 9, 48
22. Prickaerts P, Adriaens ME, Beucken Tvd et al (2016) Hypoxia increases genome-wide bivalent epigenetic marking by specific gain of H3K27me3. Epigenetics Chromatin 9, 46
23. Bock C, Kiskinis E, Verstappen G et al (2011) Reference maps of human ES and iPS cell variation enable high-throughput characterization of pluripotent cell lines. Cell 144, 439-452
24. Liang G and Zhang Y (2013) Embryonic stem cell and induced pluripotent stem cell: an epigenetic perspective. Cell Res 23, 49-69
25. Landt SG, Marinov GK, Kundaje A et al (2012) ChIP-seq guidelines and practices of the ENCODE and modENCODE consortia. Genome Res 22, 1813-1831
26. Lun DS, Sherrid A, Weiner B, Sherman DR and Galagan JE (2009) A blind deconvolution approach to high-resolution mapping of transcription factor binding sites from ChIP-seq data. Genome Biol 10, R142
27. Cremona MA, Sangalli LM, Vantini S et al (2015) Peak shape clustering reveals biological insights. BMC Bioinformatics 16, 349
28. Anzawa H, Yamagata H and Kinoshita K (2020) Theoretical characterisation of strand cross-correlation in ChIP-seq. BMC Bioinformatics 21, 417
29. Mendenhall EM, Koche RP, Truong T et al (2016) GC-Rich sequence elements recruit PRC2 in mammalian ES cells. PLoS Genet 6, e1001244
30. Thompson MD and Byrd AK (2025) Untargeted CUT&Tag reads are enriched at accessible chromatin and restrict identification of potential G4-forming sequences in G4-targeted CUT&Tag experiments. Nucleic Acids Res 53, gkaf678
31. Song MJ, Kim M, Seo J et al (2025) Role of histone modification in chromatin-mediated transcriptional repression in protozoan parasite Trichomonas vaginalis. BMB Rep 58, 82-88
32. Ai S, Yu X, Li Y et al (2017) Divergent requirements for EZH1 in heart development versus regeneration. Circ Res 121, 106-112
33. Gracia-Diaz C, Zhou Y, Yang Q et al (2023) Gain and loss of function variants in EZH1 disrupt neurogenesis and cause dominant and recessive neurodevelopmental disorders. Nat Commun 14, 4109
34. Yoon JG, Lim SK, Seo H et al (2024) De novo missense variants in HDAC3 leading to epigenetic machinery dysfunction are associated with a variable neurodevelopmental disorder. Am J Hum Genet 111, 1588-1604
35. Yu H, Hong J, Shin DY and Lee CH (2025) The role of ASXL1, SRSF2, and EZH2 mutations in chromatin dysregulation of myelodysplastic neoplasia and acute myeloid leukemia. Leukemia 39, 2329-2339
36. Bodor C, O'Riain C, Wrench D et al (2011) EZH2 Y641 mutations in follicular lymphoma. Leukemia 25, 726-729
37. Stafford JM, Lee CH, Voigt P et al (2018) Multiple modes of PRC2 inhibition elicit global chromatin alterations in H3K27M pediatric glioma. Sci Adv 4, eaau5935
38. Yap DB, Chu J, Berg T et al (2011) Somatic mutations at EZH2 Y641 act dominantly through a mechanism of selectively altered PRC2 catalytic activity, to increase H3K27 trimethylation. Blood 117, 2451-2459
39. Lee KH, Kim J and Kim JH (2024) 3D epigenomics and 3D epigenopathies. BMB Rep 57, 216-231
40. Kim H, Kim D-G, Ha S et al (2025) EZH1 Q571R-mediated chromatin compaction and its oncogenic potential in thyroid cancer. bioRxiv 2025.05.06.652476 [preprint]